Korean J. Chem. Eng., 38(6), 1179-1187 (2021)
DOI: 10.1007/s11814-021-0763-y

pISSN: 0256-1115
eISSN: 1975-7220

Reactivity of sulfur compounds in FCC decant oils for hydrodesulfurization over $CoMoS_2/Al_2O_3$ catalysts

Jihyun Kim, Jung-Geun Jang, and Yong-Kul Lee†

Laboratory of Advanced Catalysis for Energy and Environment, Department of Chemical Engineering, Dankook University, 152 Jukjeonro, Yongin 16890, Korea
(*Received 16 November 2020 • Revised 8 February 2021 • Accepted 8 February 2021*)

Abstract−$CoMoS_2/Al_2O_3$ catalysts prepared by adding citric acid (CA) were synthesized and applied tor hydrodesulfurization (HDS) of fluid-catalytic cracking decant-oils (FCC-DO). The HDS of FCC-DO was carried out in an autoclave batch reactor at 653 K and 9.4 MPa H_2. The structural properties of the catalysts were characterized by N_2 physisorption, X-ray absorption fine structure spectroscopy (XAFS), and transmission electron microscopy (TEM). The S compounds in FCC-DO have been classified into three groups in terms of the reactivity of HDS. The Co K-edge XANES analysis confirmed the formation of the Co-Mo-S phase with the addition of CA, contributing to better activity in the HDS of FCC-DO.

Keywords: FCC Decant-oils, Citric Acid, $CoMoS_2$, HDS, XANES

INTRODUCTION

Decant-oils (DO), also known as slurry oils, are produced at the bottom of the fluidized catalytic cracking (FCC) process in a refinery. FCC-DO is a highly aromatic product composed 70-90% of aromatics that also contains 0.5-3.5% sulfur, 0.1-0.3% nitrogen, and 1-3% asphaltenes [1-3]. Since FCC-DO has a moderate molecular size and high aromaticity, it is considered as a raw material for producing needle cokes [4-7]. Also, FCC-DO is used as a feedstock for mesophase pitch to produce a carbon fiber [8,9] and raw material for carbon black [10]. The S compounds in FCC-DO are critical factors in quality control as they can cause puffing in the thermal processes for the production of carbon materials [11,12]. The S compounds in FCC-DO are thus required to be removed to obtain premium carbon materials [6,13].

As a conventional HDS catalyst, alumina-supported CoMo or NiMo has been used for treating light to middle distillates [14-16]. Over the past few decades, many researchers have continued to study catalysts that have enhanced the performance and stability of CoMo and NiMo sulfides [17-19]. More recently, the addition of citric acid in the preparation of the catalysts has shown much improvement in the catalytic activity in the HDS [20-29]. CA acts as a chelating agent and has attracted much attention due to its low cost and high solubility compared to other organic additives having similar effects on delaying the sulfidation of Co or Ni species to enable the decoration [19,21]. Moreover, Nikulshin et al. reported that CA lowers the interaction between metal and support, minimizing the Mo-O-Al bond [25]. Chen et al. confirmed that the addition of CA promoted the formation of the Co-Mo-S phase [23], in which Mo precursor and CA form Mo-CA complex, resulting in more exposed S-edge being decorated by Co [23]. As such, the various effects of CA on the supported CoMo catalyst have been reported for many years. However, most of the studies usually were applied to the HDS of model S feeds [20-23] or middle distillate feedstocks [24-28]. In this work, the S compounds in FCC-DO were carefully analyzed, and the effect of CoMo-CA catalyst on the reactivity of the S compounds in the HDS was investigated. Furthermore, the active phase of the catalyst was characterized by XANES and TEM analysis.

EXPERIMENTAL

1. Materials

The FCC-DO as a feedstock was supplied from a refinery in South Korea, and the specification is summarized in Table 1. Cobalt nitrate hexahydrate ($Co(NO_3)_2{\cdot}6H_2O$, Kanto chemical, 99.5%) and ammonium molybdate tetrahydrate ($(NH_4)_6Mo_7O_{24}{\cdot}4H_2O$, Samchun chemical, 99.0%) were employed as precursors to prepare catalyst samples. The citric acid (CA) anhydrous ($C_6H_8O_7$, Samchun chemical, 99.5%) was used as a chelating agent. Alumina pellets (γ-Al_2O_3, Alfa Aesar,

Table 1. Specification of FCC-DO

Physical properties		FCC-DO
S/ppm		11,310
N/ppm		2,302
Aromatics/wt%	Total	73.78
	Mono	0.16
	Di	2.86
	Tri	27.26
	Tetra	33.99
Asphaltene/wt%		3.18
Distillation/°C	IBP/10/20	232/366/381
	30/40/50	389/398/410

†To whom correspondence should be addressed.
E-mail: yolee@dankook.ac.kr

$255\ m^2 \cdot g^{-1}$) were ground and sieved to make a uniform powder (45-75 μm) as support. Bulk Co_9S_8, and CoS_2 (Alfa Aesar, 99.5%) samples were used as XANES references [30].

2. Preparation of Supported CoMoS Catalysts

The catalysts were prepared by simultaneous incipient wetness impregnation, as previously confirmed by Valencia et al. [31], where the bimetallic sulfides prepared by co-impregnation showed a superior activity over those obtained by successive-impregnation in the HDS. Similarly, the impregnation solution was prepared with different amounts of citric acid and a constant amount of ammonium heptamolybdate tetrahydrate and cobalt nitrate to obtain the amount of metal loadings of 3 wt% Co and 10 wt% Mo, and the molar CA/Mo ratio of 0 and 1.0. After the pore volume impregnation was completed, the mixture was dried overnight at 353 K and calcined at 673 K for 4 h. Note that the CA-added catalysts were not calcined in order to keep the chelating agent in its initial form.

3. Characterization of Catalysts

N_2 adsorption-desorption isotherms of the sample were measured on a Micromeritics ASAP 2060 micropore size analyzer. The surface area of the sample was obtained by the linear portion of BET plots (P/P_0=0.01-0.14) at 77 K. Transmission electron microscope (TEM) images were obtained using a JEOL JEM-2010 electron microscope operating at 200 kV. Samples were prepared by dipping a carbon-coated copper grid into the solution containing catalyst powders in hexane. The average particle size was obtained from the TEM image over 150 particles per sample using the image analysis program, Image J 1.50i.

The X-ray absorption near-edge structure spectroscopy (XANES) spectra at the Co K-edge (7.709 keV) for the catalyst samples were measured using synchrotron radiation at the beamline 8C of the Pohang Light Source (PLS). The X-ray ring at the PLS has a flux of 2×10^{12} photons s^{-1} at 360 mA and 3.0 GeV. The X-ray single crystal at the beamline 8C is equipped with a Si (1 1 1) channel-cut monochromator and has an energy range capability of 4-22 keV. The samples were prepared by placing the slurry catalysts on the Kapton-sealed cell. Background removal and normalization of the XANES spectra were obtained using XAFS analysis program Winxas 3.1.

4. Catalytic Activity Tests for HDS of FCC-DO

The catalytic activity test for HDS of FCC-DO was conducted after the in-situ sulfidation of the catalyst using 1 wt% dimethyldisulfide (DMDS, Alfa Aesar) in n-hexadecane (Alfa Aesar) at 673 K and 6.0 MPa H_2. After venting, the reactor was charged with FCC-DO of 30 g and purged with H_2 for three times to fill 6.0 MPa with H_2 (at 353 K). Thereafter, the reactor was heated to 653 K with a temperature ramping rate of $10\ K \cdot min^{-1}$, and the H_2 pressure was increased to 9.4 MPa. After the reaction test, the reactor was cooled to 353 K, and the gaseous products were vented. The liquid product samples were collected manually, and the remaining products were washed in toluene and centrifuged for 0.5 h to separate precipitate products, including the catalyst. For a gas chromatographic (GC) analysis, FCC-DO feedstock and the liquid products were dissolved at 10 wt% in toluene with 15 ppm of benzothiophene (BT) as standard. Diluted samples were identified with an Agilent 6890 N GC, equipped with a flame ionization detector (FID) and DB-1 (Hewlett Packard, dimethylpolysiloxane, 0.25 mm i.d.×30 m), and samples were identified by matching retention times with commercially available standards as well as by GC-MS analysis. The GC-MS consisted of Agilent 6890 N GC, equipped with an Agilent 5973 mass selective detector (GC-MS) and DB-1MS (Hewlett Packard, dimethylpolysiloxane, 0.25 mm i.d.×30 m).The sulfur compounds were quantified by using a GC equipped with a sulfur chemiluminescence detector (GC-SCD). The GC-SCD consisted of Agilent 6890 N GC equipped with HP-5 column (Hewlett Packard, 5% phenyl-methylpolysiloxane, 30 m×0.32 mm i.d.).

RESULTS AND DISCUSSION

1 Sulfur Compounds in FCC-DO

Fig. 1 shows GC-SCD chromatographs of the feedstock, FCC-DO, and the corresponding S compounds are listed in Table 2. As can be seen, the S compounds are mostly composed of dibenzothiophene-derivatives and thus can be categorized in terms of the number of alkyl substitutions. For example, dibenzothiophene (DBT) accounts for 0.9 wt% of total S in FCC-DO, followed by C1-DBT of 4.8, C2-DBT of 10.7, C3-DBT of 19.1, C4-DBT of 21.3, and benzonaphthothiophene (BNT)-derivatives of 35.9 wt%. Similar results were also reported by Eser et al., where DBT- and BNT-derivatives were quantified as much as 65 and 35%, respectively [32,33]. Among C1-DBT compounds, the amount of 4-MDBT was highest of 1.73 wt%, followed by 2-/3-MDBT of 1.69 wt%, and 1-MDBT of 0.55 wt%. Among C2-DBT compounds, the amount of 2,6-/3,6-DMDBT was highest of 2.80 wt%, followed by 1,3-DMDBT (1.25)>

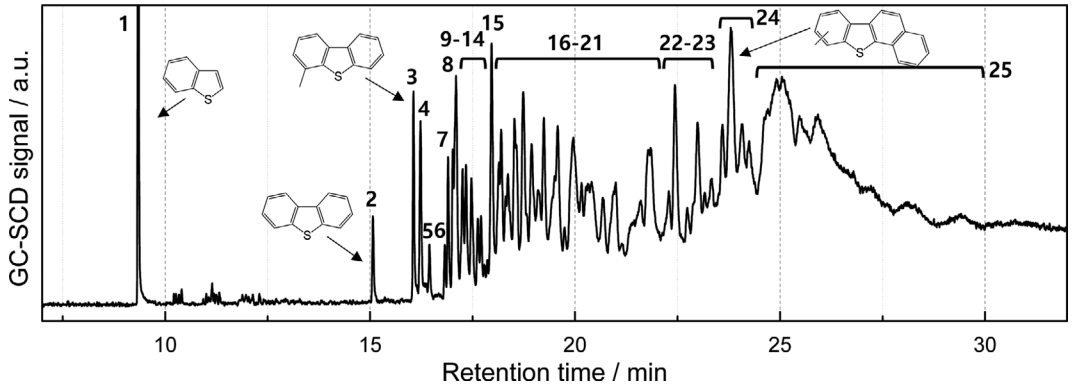

Fig. 1. GC-SCD chromatograph of FCC-DO.

Table 2. Composition of sulfur compounds in FCC-DO

No	S compounds	Formula	Composition/ppm	S fraction/%
1	Benzothiophene	C_8H_6S	-	-
2	Dibenzothiophene	$C_{12}H_8S$	102	0.9
3	4-Methyl dibenzothiophene	$C_{13}H_{10}S$	196	1.73
4	2-/3-Methyl dibenzothiophene	$C_{13}H_{10}S$	191	1.69
5	1-Methyl dibenzothiophene	$C_{13}H_{10}S$	62	1.69
6	4-Ethyl dibenzothiophene	$C_{14}H_{12}S$	46	0.55
7	4,6-Dimethyl dibenzothiophene	$C_{14}H_{12}S$	122	0.41
8	2,4-Dimethyl dibenzothiophene	$C_{14}H_{12}S$	117	1.08
9	2,6-/3,6-Dimethyl dibenzothiophene	$C_{14}H_{12}S$	317	1.03
10	2,8-Dimethyl dibenzothiophene	$C_{14}H_{12}S$	137	2.80
11	1,4-Dimethyl dibenzothiophene	$C_{14}H_{12}S$	137	1.21
12	Dimethyl dibenzothiophene	$C_{14}H_{12}S$	141	1.21
13	2,3-Dimethyl dibenzothiophene	$C_{14}H_{12}S$	77	1.25
14	Trimethyl dibenzothiophene	$C_{15}H_{14}S$	67	0.59
15	2,4,6-Trimethyl dibenzothiophene	$C_{15}H_{14}S$	294	2.60
16	Trimethyl dibenzothiophene	$C_{15}H_{14}S$	107	0.95
17	Trimethyl dibenzothiophene	$C_{15}H_{14}S$	136	1.20
18	Trimethyl dibenzothiophene	$C_{15}H_{14}S$	17	0.15
19	3,4,6-Trimethyl dibenzothiophene	$C_{15}H_{14}S$	126	1.11
20	Trimethyl dibenzothiophene	$C_{15}H_{14}S$	1,055	9.33
21	Tetramethyl dibenzothiophene	$C_{16}H_{16}S$	2,405	21.26
22	Benzo[b]naphtho[2,1-d]thiophene	$C_{16}H_{10}S$	308	2.72
23	Benzo[b]naphtho[1,2-d]thiophene	$C_{16}H_{10}S$	260	2.29
24	Methyl benzonaphthothiophene	$C_{17}H_{12}S$	1,242	10.04
25	Dimethyl benzonaphthothiophene	$C_{18}H_{14}S$	2,249	19.89

2,8-/1,4-DMDBT (1.21)>4,6-DMDBT (1.08)>2,4-DMDBT (1.04)> 2,3-DMDBT (0.68)>1,2-DMDBT (0.60). For C3-DBT compounds, the amount of 2,4,6-TMDBT was highest of 2.60 wt%, followed by 1,4,6-TMDBT (1.20)>3,4,6-TMDBT (1.11)>2,4,8-/2,4,7-TMDBT (0.95)>1,4,8-TMDBT (0.15). For BNT-derivatives, C1-BNT was dominant with 10.1 wt% of total BNT-derivatives of 35.9 wt%.

2. Reactivity of S Compounds of FCC-DO in HDS over CoMoS Catalyst

Fig. 2 displays distributions of S-compounds before and after the HDS of FCC-DO over CoMoS catalyst. After the HDS, although the total S content was decreased from 11,310 ppm S to 7,216 ppm S with an overall HDS conversion of 36.2%, the remaining S fractions of the S compounds were found different from those in the original feed. For example, the DBT underwent a relatively high HDS conversion of 54.9%, even higher than the overall HDS conversion, resulting in a decreased fraction from 0.9 to 0.6% of total S compounds remaining after the HDS. In contrast, the 4-MDBT experienced a relatively low HDS conversion of 10.2%, even lower than the overall HDS conversion, leading to an increased fraction from 1.73 to 2.43% of total S compounds remaining after the HDS. More importantly, the 4,6-DMDBT, known as the most refractory S compound in petroleum feedstocks, experienced the lowest HDS conversion of 1.6%, even lower than that of 4-MDBT, being more than doubled in the fraction from 1.08 to 2.43% of total S compounds remaining after the HDS. These results thus suggest that it would be more desirable to categorize the S-compounds in the FCC-DO depending on reactivity rather than molecular weight or structures. For S-compounds in gas oils as a diesel pool, Mochida group proposed four groups that were categorized based upon the reactivity in HDS [1,8,34]. For example, the representative S compounds are benzothiophenes, dibenzothiophene (DBT), 4-methyl-DBT (4-MDBT), and 4,6-dimethyl-DBT (4,6-DBDBT), corresponding to Group I, II, III, and IV, respectively. In a similar manner, the reactivity of the S-compounds FCC-DO in the HDS was compared at the given reaction condition. The amount of the representative S compounds of DBT (Group II), 4-MDBT (Group III), and 4,6-DMDBT (Group IV) was compared before and after the HDS over CoMoS catalyst at 9.4 MPa and 653 K. Again, the original S fraction of the representative S compounds is 0.90 wt% for DBT, 1.73 wt% for 4-MDBT, and 1.08wt% for 4,6-DMDBT. For the other S compounds, the respective HDS conversion and the remaining fraction were compared as listed in Table 3. Overall, the S-compounds can be categorized into three groups in terms of reactivity in the HDS. The S-compounds that belong to group II are sterically less-hindered DBT and alkyl-substituted DBTs such as 1-/2-/3-MDBT, and 2,8-/2,3-DMDBT, which show a similar reactivity in the HDS with DBT, leading to a lower remaining S fraction than those of the original feedstock. The S-compounds that belong to group III are partially hindered 4-MDBT and its alkyl-substituted 4-MDBTs such as 2,4-/1,4-DMDBT, and 2,4,8-/2,4,7-/1,4,8-TMDBT. The S-compounds that belong to group IV are severely hindered 4,6-DMDBT and its alkyl-substituted ones such as 2,4,6-/3,4,6-

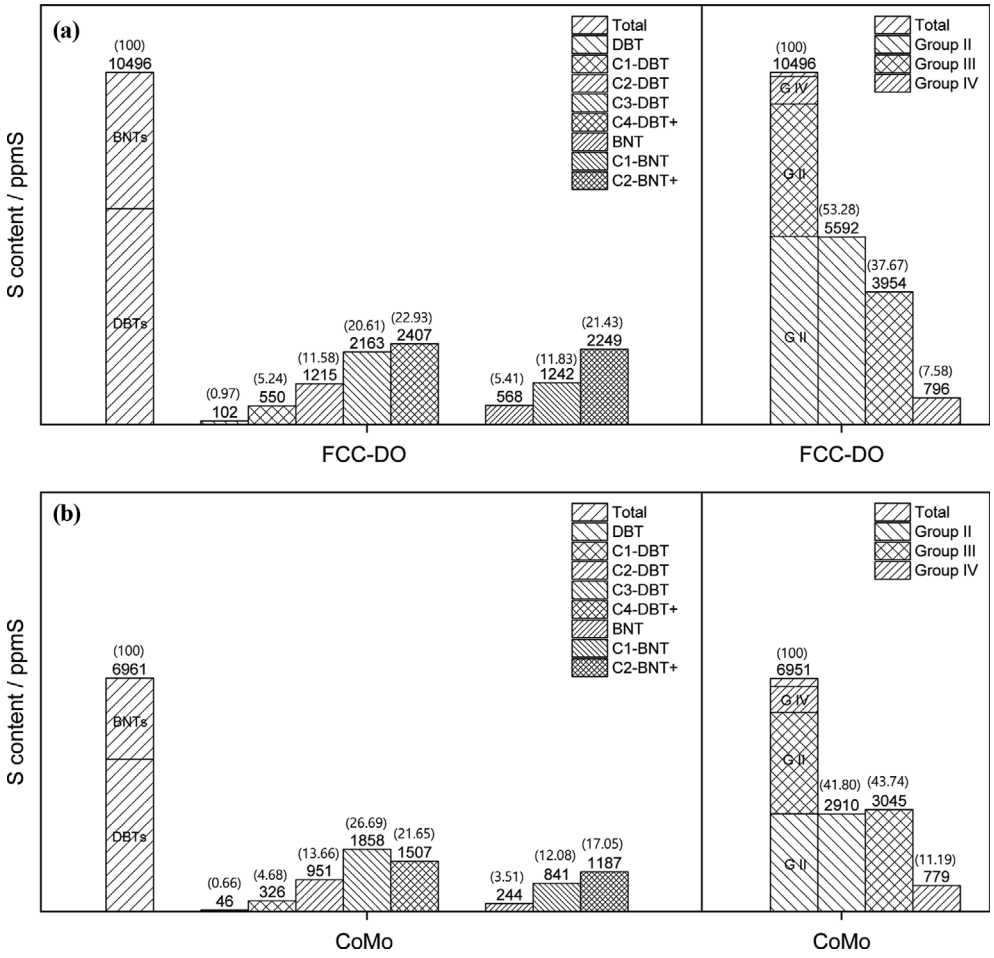

Fig. 2. Contents of S compounds by molecular types and reactivity in HDS: (a) FCC-DO; (b) treated product after HDS over CoMo catalyst.

Table 3. Comparison of reactivity of S compounds of FCC-DO in HDS

	[a]Total HDS conversion/%	[b]Group II HDS conversion/%		[c]Group III HDS conversion/%		[d]Group IV HDS conversion/%	
		DBT	Total S in Group II	4-MDBT	Total S in Group III	4,6-DMDBT	Total S in Group IV
CoMo	36.2	54.90	47.96	10.20	22.99	1.64	2.14
CoMo-CA	44.3	71.57	59.12	11.22	29.72	1.64	2.64

[a]Total HDS conversion (%) $= \left[1 - \frac{\text{Sulfur in product (wt\%)}}{\text{Sulfur in feed (wt\%)}}\right] \times 100$

[b]Group II HDS conversion (%) $= \left[1 - \frac{\text{GroupII in product (wt\%)}}{\text{GroupII in feed (wt\%)}}\right] \times 100$

[c]Group III HDS conversion (%) $= \left[1 - \frac{\text{GroupIII in product (wt\%)}}{\text{GroupIII in feed (wt\%)}}\right] \times 100$

[d]Group IV HDS conversion (%) $= \left[1 - \frac{\text{GroupIV in product (wt\%)}}{\text{GroupIV in feed (wt\%)}}\right] \times 100$

TMDBT. Again, as displayed in Fig. 2, the S-compounds of group II show a relatively high reactivity in the HDS, resulting in a lower fraction after the HDS. In contrast, the S-compounds of group III led to an increased fraction by no more than 50% from the original feedstock to those the product. The most hindered S-compounds, group IV, were found to remain almost unreacted after the HDS.

3. Effect of a Better CoMoS Catalyst on the Reactivity of S Compounds

Considering the low conversion of the S-compounds of FCC-DO in the HDS, it is required to increase the reactivity of the S-compounds. In this regard, a better CoMoS catalyst was prepared to

Table 4. Physical properties of catalyst samples

	BET surface area/m^2g^{-1}	Pore volume/cm^3g^{-1}	Average pore size/nm
CoMo	226.08	0.476	4.80
CoMo-CA	186.63	0.454	4.46

apply for the HDS of FCC-DO. The active phase of the $CoMoS/Al_2O_3$ catalyst is related to the interaction between the support and CoMoS catalyst. The Co-Mo-S type I, showing a stronger interaction with support, is known to form a highly dispersed monolayer structure, while the Co-Mo-S type II, featuring a lower interaction with support, appears in a multilayer form [16]. Moreover, the location of Co species that is known to be anchored on the lateral sites of MoS_2 slabs is of great importance in the formation of the active Co-Mo-S phase. In preparing a highly active CoMoS catalyst, the effect of citric acid (CA) addition on the HDS was well established in previous studies [26-29]. The addition of CA plays a crucial role in the formation of the Co-Mo-S phase and is also known to affect the slab size and stacking number of $CoMoS_2$ catalysts [21,23,29]. Table 4 summarizes the physical properties of the catalyst samples. The BET surface area of fresh catalyst samples decreased with the addition of CA. This is because the added CA forms a metal complex, residing on the surface of the catalyst. A previous study by Peña et al. also confirmed a similar physical change in the CA-added CoMo/SBA-15 catalyst [20].

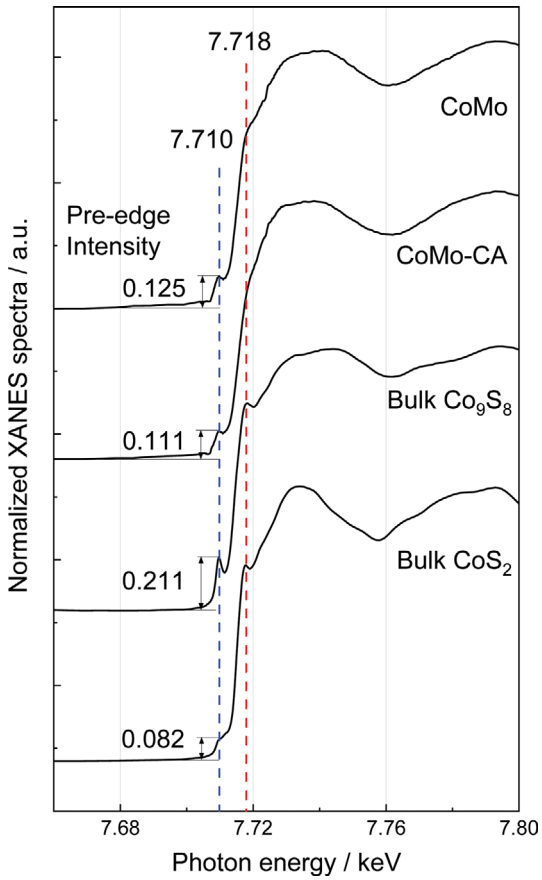

Fig. 3. The Co K-edge XANES spectra of CoMo, CoMo-CA, and bulk references.

Fig. 3 shows the Co K-edge XANES spectra of CoMo, CoMo-CA, and bulk CoSx references. The XANES spectrum for the reference Co_9S_8 shows a strong pre-edge peak at 7.710 keV with a shoulder at 7.718 keV, corresponding to the 1s→3d and 1s→3p transitions, respectively [30,35,36]. On the contrary, the spectrum for CoS_2 shows a weak pre-edge peak. These results can be explained by the local structure of Co species. The strong pre-edge intensity of Co_9S_8 is a typical property of the tetrahedral Co site. The unit cell of Co_9S_8 (Fm-3m) is composed of eight tetrahedral Co sites, whereas the CoS_2 (Pa-3) consists of only octahedral Co sites [36,37]. The XANES spectrum of the CoMo sample appears very similar to that of CoS_2 but with slightly high intensity, indicating the coexistence of Co_9S_8 in the catalyst. In contrast, the CoMo-CA shows a weak pre-edge peak in the XANES spectrum, revealing the Co phase being different from Co_9S_8. Previous work by Prins et al. reported an octahedral-like coordinated Co species in the Co-Mo-S phase [36] on CoMoS ($\bar{1}$ 0 1 0) edge and this was recently proved by Lauritsen et al. using STM analysis [38]. These results suggest that the introduction of CA affects the formation of the Co-Mo-S phase. These results are in line with our previous study on the unsupported $CoMoS_2$ catalysts, where a DFT calculation on the $CoMoS_2$ catalysts and EXAFS analysis also confirmed the formation of Co-Mo-S phase on the edge-sites of MoS_2 being decorated by Co species [30].

TEM images of the catalysts collected after the HDS of FCC-DO are given in Fig. 4. It is observed that catalyst particles were formed with an average length of 4.5 nm for CoMo. The CoMo-CA catalyst showed smaller particle size distributions with an average length of 4.0 nm. Castillo-Villalón et al. also obtained similar results on the particle size with the use of CA [22]. The addition of a small amount of CA decreased the particle size and increased the dispersion of the catalyst without the increase of the average stacking numbers. These results indicate that the addition of CA allowed smaller and more dispersed $CoMoS_2$ particles with the formation of the Co-Mo-S phase.

Figs. 5 and 6 compare the S distribution of the feed and the products after the HDS over CoMo and CoMo-CA catalysts. It is obvious that the CoMo-CA showed better activity in the HDS of FCC-DO than the CoMo catalyst with the total S conversion of 44.3 and 36.2%, respectively. Taking into account the reactivity of the S compounds in the HDS, it can be noted that BNT derivatives show a higher HDS conversion than C2- or C3-DBTs, indicating that the reactivity in the HDS is not just dependent on the size of the molecules.

The S compounds in the feed and the products after the HDS were categorized by three groups depending on the HDS reactivity, as given in Table 5 and Fig. 7. The S compounds of FCC-DO are composed of 54.0% of Group II, 38.2% of Group III, and 7.7% of Group IV. The fraction of the S-compounds of each group remaining after the HDS turned out be 43.2, 45.2, and 11.5%, respectively,

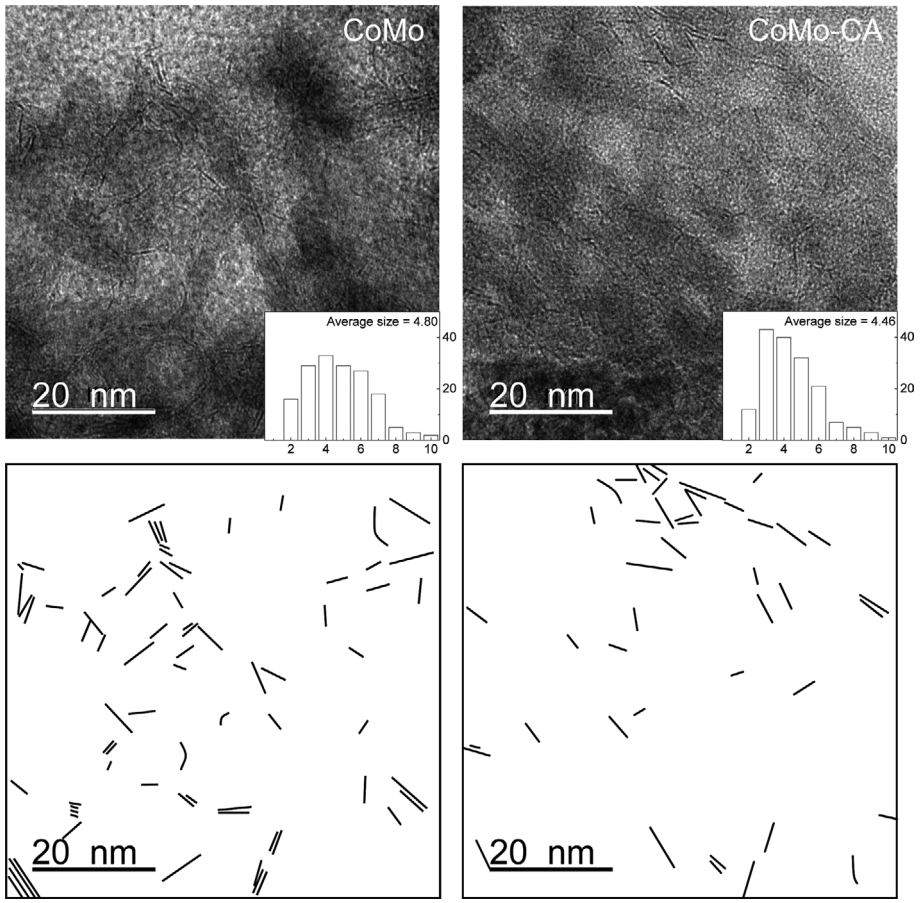

Fig. 4. TEM image of CoMo and CoMo-CA catalysts.

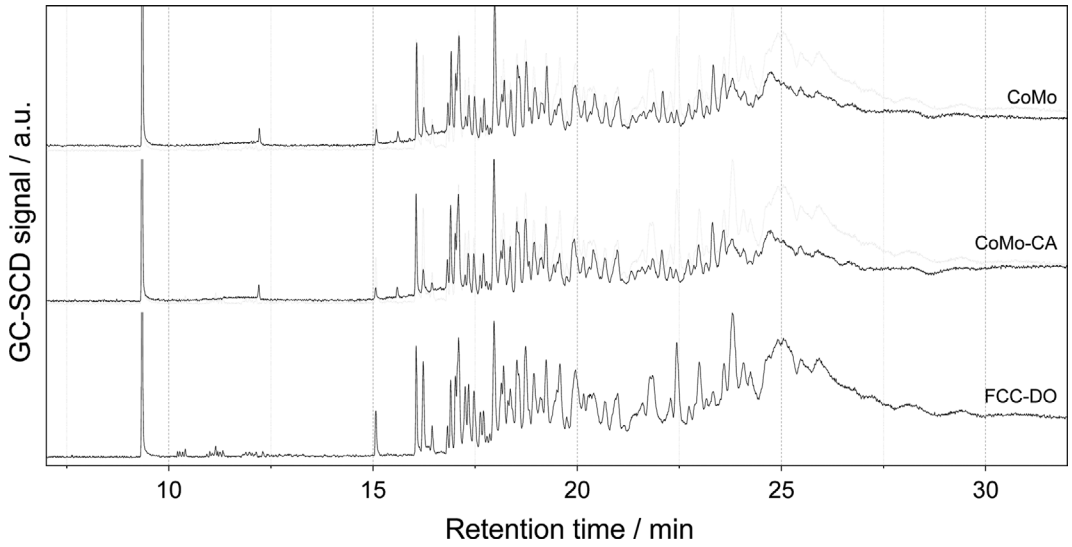

Fig. 5. GC-SCD chromatographs of HDS products over CoMo and CoMo-CA catalysts.

over CoMo catalyst, and 39.1, 47.6, and 13.2%, respectively, over CoMo-CA. These results indicate that most parts of the S removal took place in group II, while only a slight decrease in the S content was observed for group III. Nonetheless, S-compounds in group IV remained almost unchanged. These results again indicate that the CoMo catalyst effectively lowered the S compounds that are less sterically hindered while showing a low activity toward the refractory S-compounds belonging to groups III and IV. This can be explained by the nature of the catalytic activity of $CoMoS_2$ in the HDS, favoring the HDS via the direct desulfurization pathway. Again, the HDS

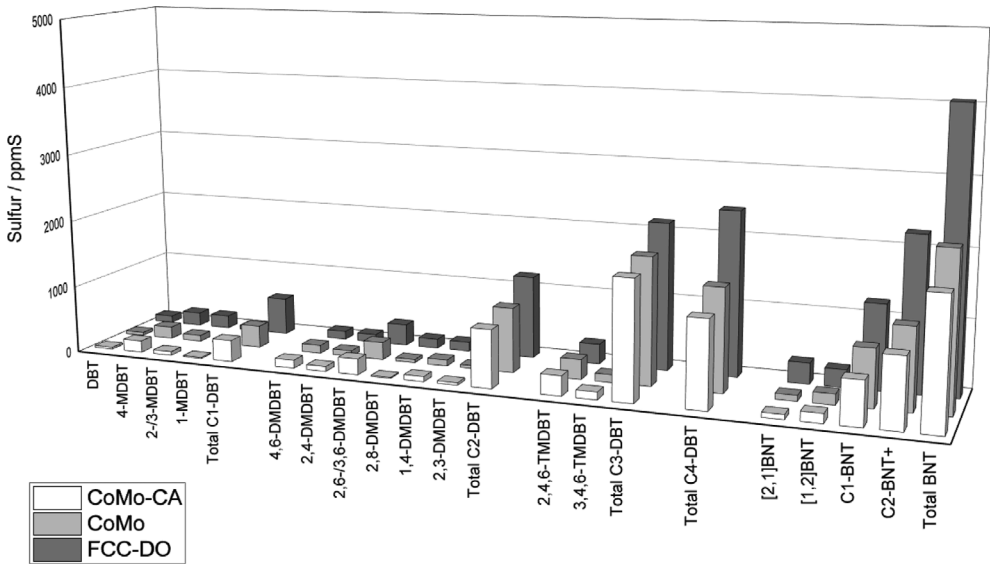

Fig. 6. Distributions of S compounds before and after HDS over CoMo and CoMo-CA catalysts.

Table 5. Composition of S compounds before and after HDS

Compound	FCC-DO		CoMo		CoMo-CA		S Group
	ppm	Fraction/%	ppm	Fraction/%	ppm	Fraction/%	
Total	11,310		7,216		6,300		
DBT	102	0.97	46	0.66	29	0.48	II
4-MDBT	196	1.87	176	2.53	174	2.85	III
2-/3-MDBT	191	1.82	90	1.29	56	0.92	II
1-MDBT	62	0.59	27	0.39	16	0.26	II
Total C1-DBT	550	5.24	326	4.68	321	5.26	
4,6-DMDBT	122	1.16	120	1.72	120	1.97	IV
2,4-DMDBT	117	1.11	84	1.21	75	1.23	III
2,6-/3,6-DMDBT	317	3.02	259	3.72	236	3.87	III
2,8-DMDBT	137	1.31	49	0.70	15	0.25	II
1,4-DMDBT	137	1.31	90	1.29	77	1.26	II
2,3-DMDBT	77	0.73	44	0.63	37	0.61	II
Unidentified S-1	255	2.43	211	3.03	210	3.44	III
Total C2-DBT	1,215	11.58	951	13.66	853	13.99	
2,4,6-TMDBT	294	2.80	293	4.21	292	4.79	IV
3,4,6-TMDBT	126	1.20	115	1.65	114	1.87	IV
Unidentified S-2	446	4.25	288	4.14	224	3.67	II
Unidentified S-3	1,043	9.94	812	11.66	767	12.58	III
Unidentified S-4	254	2.42	250	3.59	249	4.08	IV
Total C3-DBT	2,163	20.61	1,858	26.69	1,746	28.63	
Unidentified S-5	1,694	16.14	939	13.49	732	12.00	II
Unidentified S-6	713	6.79	568	8.16	545	8.94	III
Total C4-DBT	2,407	22.93	1,507	21.65	1,278	20.96	
[2,1]BNT	308	2.93	86	1.24	72	1.18	II
[1,2]BNT	260	2.48	158	2.27	141	2.31	II
C1-BNT	1,242	11.83	841	12.08	643	10.54	
C2-BNT+	2,249	21.43	1,187	17.05	1,015	16.64	
Unidentified S-7	2,315	22.06	1,184	17.01	963	15.79	II
Unidentified S-8	1,176	11.20	844	12.12	695	11.40	III
Total BNT	4,059	38.67	2,273	32.65	1,871	30.68	

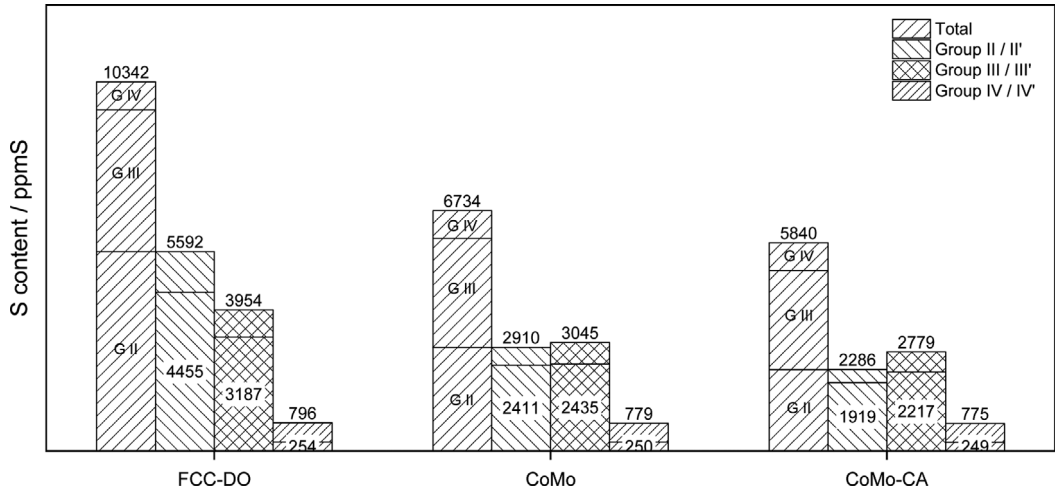

Fig. 7. Sulfur compounds distribution by reactivity in HDS: Goup II′, III′, IV′ are unnidentified S compounds in the respective group.

of the sulfur compounds occurs through two routes: hydrogenation (HYD) and direct desulfurization (DDS) [16]. The S compounds of FCC-DO are mostly composed of large molecules such as dibenzothiophene (DBT), alkyl-DBTs, and benzonaphthothiophene's (BNT)-derivatives, of which C-S bonds are difficult to break due to the strong steric hindrance [17]. Nonetheless, the presence of alkyl substitutions on C4 or C6 positions of DBT makes the DDS pathway more difficult, as the σ-adsorption between S and active center of the catalyst that is an initial step of the DDS route is sterically hindered [16]. The HYD pathway effectively alleviates the steric hindrance by saturating one of the DBT's aromatic rings, facilitating the following HDS [13]. This is an ongoing work to lessen the steric hindrance of the S compounds of FCC-DO to fasten the HDS, which can be achieved by promoting the HYD activity, particularly over $NiMoS_2$ catalysts.

CONCLUSIONS

The HDS of FCC-DO was conducted in an autoclave batch reactor at 653 K and 9.4 MPa H_2. The S compounds of FCC-DO were classified into three groups according to the reactivity in the HDS, from the highest active group of sterically less hindered alkyl-DBTs to the lowest active group of sterically hindered DBT-derivatives. It was identified that citric acid added-$CoMoS_2$ catalysts (CoMo-CA) were successfully prepared and applied to the HDS of FCC-DO and showed better activity than CoMo. TEM images confirmed that the addition of CA leads to a decrease of average particle size of $CoMoS_2$ slab down to 4.0 nm. Furthermore, the formation of the Co-Mo-S phase was identified by the Co K-edge XANES analysis particularly featuring a weak pre-edge intensity due to an octahedral-coordination of Co-Mo-S phase. Overall, it was concluded that the addition CA in the preparation of CoMo sulfides contributes to the improvement of the catalytic activity in the HDS of FCC-DO via the formation of a well-dispersed Co-Mo-S phase.

ACKNOWLEDGEMENT

The authors acknowledge the financial support from the National Research Foundation of Korea (NRF-2019R1A2C2009999) and the Ministry of Trade, Industry & Energy of Korea (MOTIE-10082582).

REFERENCES

1. I. Mochida, T. Oyama and Y. Korai, *Carbon N. Y.*, **26**, 49 (1988).
2. B. Fixari, P. Belloir and P. Le Perchec, *Fuel*, **73**, 1284 (1994).
3. J. H. Kim, J. G. Kim, K. B. Lee and J. S. Im, *Carbon Lett.*, **29**, 203 (2019).
4. G. Wang and S. Eser, *Energy Fuels*, **21**, 3563 (2007).
5. E. Altamirano, J. A. de los Reyes, F. Murrieta and M. Vrinat, *Catal. Today*, **133-135**, 292 (2008).
6. M. M. Escallon, D. A. Fonseca and H. H. Schobert, *Energy Fuels*, **27**, 478 (2013).
7. R. T. Wincek, J. P. Abrahamson and S. Eser, *Energy Fuels*, **30**, 6281 (2016).
8. Y. D. Park and I. Mochida, *Carbon N. Y.*, **27**, 925 (1989).
9. S. Ko, J. Eun, C. W. Lee and Y. P. Jeon, *Carbon Lett.*, **30**, 35 (2020).
10. M.-J. Wang, C. A. Gray, S. A. Reznek, K. Mahmud and Y. Kutsovsky, *Kirk-Othmer Encyclopedia of Chemical Technology*, Wiley, New York, 761 (2004).
11. H. P. Halim, J. S. Im and C. W. Lee, *Carbon Lett.*, **14**, 152 (2013).
12. L. Edwards, *Jom*, **67**, 308 (2015).
13. J. P. Abrahamson, R. T. Wincek and S. Eser, *Energy Fuels*, **30**, 7173 (2016).
14. N. Azizi, S. A. Ali, K. Alhooshani, T. Kim, Y. Lee, J. I. Park, J. Miyawaki, S. H. Yoon and I. Mochida, *Fuel Process. Technol.*, **109**, 172 (2013).
15. M. V. Landau, *Catal. Today*, **36**, 393 (1997).
16. A. Stanislaus, A. Marafi and M. S. Rana, *Catal. Today*, **153**, 1 (2010).
17. R. Javadli and A. de Klerk, *Appl. Petrochem. Res.*, **1**, 3 (2012).
18. J. Ancheyta, *Deactivation of heavy oil hydroprocessing catalysts*, Wiley, New York (2016).
19. J. N. D. de León, C. R. Kumar, J. Antúnez-García and S. Fuentes-Moyado, *Catalysts*, **9**, 87 (2019).
20. L. Peña, D. Valencia and T. Klimova, *Appl. Catal. B Environ.*, **147**, 879 (2014).
21. S. V. Budukva, O. V. Klimov, Y. A. Chesalov, I. P. Prosvirin, T. V.

Larina and A. S. Noskov, *Catal. Lett.*, **148**, 1525 (2018).
22. P. Castillo-Villalon, J. Ramirez and J. A. Vargas-Luciano, *J. Catal.*, **320**, 127 (2014).
23. J. Chen, J. Mi, K. Li, X. Wang, E. Dominguez Garcia, Y. Cao, L. Jiang, L. Oliviero and F. Maugé, *Ind. Eng. Chem. Res.*, **56**, 14172 (2017).
24. O. V. Klimov, A. V. Pashigreva, M. A. Fedotov, D. I. Kochubey, Y. A. Chesalov, G. A. Bukhtiyarova and A. S. Noskov, *J. Mol. Catal. A Chem.*, **322**, 80 (2010).
25. P. A. Nikulshin, D. I. Ishutenko, A. A. Mozhaev, K. I. Maslakov and A. A. Pimerzin, *J. Catal.*, **312**, 152 (2014).
26. S. L. González-Cortés, Y. Qian, H. A. Almegren, T. Xiao, V. L. Kuznetsov and P. P. Edwards, *Appl. Petrochem. Res.*, **5**, 181 (2015).
27. S. V. Budukva, O. V. Klimov, D. D. Uvarkina, Y. A. Chesalov, I. P. Prosvirin, T. V. Larina and A. S. Noskov, *Catal. Today*, **329**, 35 (2019).
28. A. V. Pashigreva, G. A. Bukhtiyarova, O. V. Klimov, Y. A. Chesalov, G. S. Litvak and A. S. Noskov, *Catal. Today*, **149**, 19 (2010).
29. A. Villarreal, J. Ramírez, L. C. Caero, P. C. Villalón and A. Gutiérrez-Alejandre, *Catal. Today*, **250**, 60 (2015).
30. K.-D. Kim and Y.-K. Lee, *J. Catal.*, **380**, 278 (2019).
31. D. Valencia, I. García-Cruz and T. Klimova, *Stud. Surf. Sci. Catal.*, **175**, 529 (2010).
32. R. M. Filley and S. Eser, *Energy Fuels*, **11**, 623 (1997).
33. S. Eser and G. Wang, *Energy Fuels*, **21**, 3573 (2007).
34. X. Ma, K. Sakanishi and I. Mochida, *Ind. Eng. Chem. Res.*, **35**, 2487 (1996).
35. Y. Okamoto, K. Hioka, K. Arakawa, T. Fujikawa, T. Ebihara and T. Kubota, *J. Catal.*, **268**, 49 (2009).
36. S. M. A. M. Bouwens, D. C. Koningsberger, V. H. J. de Beer and R. Prins, *Am. Chem. Soc. Div. Pet. Chem. Prepr.*, **33**, 596 (1988).
37. L. Van Haandel, G. Smolentsev, J. A. Van Bokhoven, E. J. M. Hensen and T. Weber, *ACS Catal.*, **10**, 10978 (2020).
38. J. V. Lauritsen, M. V. Bollinger, E. Lægsgaard, K. W. Jacobsen, J. K. Nørskov, B. S. Clausen, H. Topsøe and F. Besenbacher, *J. Catal.*, **221**, 510 (2004).